

apter]schemelosScheme

**University of São Paulo
São Carlos School of Engineering**

Guilherme Soares Silvestre

**Robotic-Assisted SEEG for Epilepsy: A Phantom-Based
Accuracy Study of the Yara Platform**

**São Carlos
2025**

Guilherme Soares Silvestre

Robotic-Assisted SEEG for Epilepsy: A Phantom-Based Accuracy Study of the Yara Platform

Final project presented to the Mechatronics Engineering Course, at the São Carlos School of Engineering, University of São Paulo, as part of the requirements to obtain the title of Mechatronics Engineer.

Advisor: Prof. Dr. Glauco Augusto de Paula Caurin

**São Carlos
2025**

ACKNOWLEDGEMENTS

I gratefully acknowledge Prof. Glauco Caurin for his supervision, methodological guidance, and encouragement. His expertise and his substantive feedback were essential to the conception, execution, and refinement of this research. I also thank Prof. Hélio Machado and Prof. Marcelo Volpon for contributing essential medical knowledge and clinical insight, which informed the experimental design, data interpretation, and validation.

I am grateful to M.Sc. Allison da Silva for technical assistance during data acquisition, including operating-room organization, electrode placement, and the procedures used to assess measurement accuracy. I acknowledge my friends and BMT co-founders for their collaboration and vision of bringing technology to world healthcare.

I also thank my aunt, my uncle, and my cousins for their assistance during the university admission process. Finally, I express my profound gratitude to my mother, my father, my brother, and my girlfriend for their sustained support, patience, and encouragement throughout the entire graduate program.

He who has a why to live can bear almost any how.

Friedrich Nietzsche

ABSTRACT

Silvestre, G.S. Robotic-Assisted SEEG for Epilepsy: A Phantom-Based Accuracy Study of the Yara Platform. 2025. 47p. Monograph (Conclusion Course Paper) - University of São Paulo, São Carlos, 2025.

This work evaluates the accuracy of the Yara collaborative robotic platform for intracranial electrode placement in stereoelectroencephalography (SEEG) procedures. SEEG is a minimally invasive technique used in epilepsy surgery, requiring precise electrode implantation to localize epileptogenic zones. The study introduces custom-designed cranial phantoms that replicate human anatomical structures, enabling controlled experiments to assess the technical performance of the robotic system. Accuracy validation is performed in both in-lab mock operating room (mock-OR) and operating room (OR) environments. Results demonstrate that the Yara system achieves placement errors comparable to established robotic platforms, with average target point error (TPE) of 1.8 mm in conical target phantom tests, entry point error (EPE) of 1.3 mm and TPE of 3.07 mm in synthetic brain phantom in mock-OR, EPE of 3.1 mm and TPE 5.8 mm in OR evaluation. The findings highlight the potential of collaborative robotics to enhance precision and efficiency in SEEG procedures, supporting future clinical applications in epilepsy surgery.

Keywords: Robotic Neurosurgery, Epilepsy Surgery, Collaborative Robotics, Cranial Phantom

RESUMO

Silvestre, G.S. Robotic-Assisted SEEG for Epilepsy: A Phantom-Based Accuracy Study of the Yara Platform. 2025. 47p.

Este trabalho avalia a exatidão da plataforma robótica colaborativa Yara para posicionamento de eletrodos intracranianos em procedimentos de estereoeletroencefalografia (SEEG). SEEG é uma técnica minimamente invasiva usada em cirurgia de epilepsia, exigindo implantação precisa de eletrodos para localizar zonas epileptogênicas. O estudo apresenta *phantom* cranianos que replicam estruturas anatômicas humanas, permitindo experimentos controlados para avaliar o desempenho técnico do sistema robótico. A validação da precisão é realizada em ambientes de laboratório e centro cirúrgico. Os resultados demonstram que o sistema Yara atinge erros de posicionamento comparáveis aos de plataformas robóticas estabelecidas, com erro médio no ponto-alvo (TPE) de 1,8 mm em testes com *phantom* com alvos cônicos, erro no ponto de entrada (EPE) de 1,3 mm e TPE de 3,07 mm em *phantom* com cérebro sintético em ambiente simulado (SE), EPE de 3,1 mm e TPE de 5,8 mm em testes em centro cirúrgico. Os resultados destacam o potencial da robótica colaborativa e a eficiência em procedimentos de SEEG, apoiando futuras aplicações clínicas em cirurgia de epilepsia.

Monografia (Trabalho de Conclusão de Curso) - University of São Paulo, São Carlos, 2025.

Palavras-chave: Robotic Neurosurgery, Epilepsy Surgery, Collaborative Robotics, Cranial Phantom.

LIST OF FIGURES

Figure 1 – Positioning of electrodes in scalp EEG, subdural EEG (SDE), and SEEG procedures respectively (SHEN, 2020) (Blausen.com staff, 2014) (JONES <i>et al.</i> , 2018)	24
Figure 2 – (a) presents Talairach’s frame with x-ray supports and (b) presents an example x-ray image alongside the coordinate system developed by Talairach (MAZOYER, 2008)	25
Figure 3 – Frame Leksell G without N-Localizer and with N-Localizer respectively (ROJAS-VILLABONA <i>et al.</i> , 2016)	25
Figure 4 – Robots capable of performing SEEG surgeries: Zimmer Biomet ROSA ONE Brain, Brainlab Cirq and Renishaw Neuromate respectively.	28
Figure 5 – Conical targets phantom used for quantitative accuracy assessment via stereoscopic imaging.	36
Figure 6 – Conical targets phantom in SE for metal rods positioning using the robotic system.	36
Figure 7 – Examples of stereo camera images used to measure the distance between the metal rod tip and the planned target point. The top and bottom rows show the left and right images of a stereo pair for the same moment in time.	37
Figure 8 – Phantom model with synthetic brain produced using silicone rubber and 3D printed plastic surface skin after electrode placement.	37
Figure 9 – Synthetic brain phantom in mock-OR during electrode placement with the robotic system. The rightmost image displays the postoperative CT scan of inserted electrodes.	38
Figure 10 – Comparison between preoperative (red and green lines) and postoperative (gray contacts) electrode trajectories using CT scan of the synthetic brain model in the mock-OR.	39
Figure 11 – Phantom model with synthetic brain placed in the OR using stereotactic frame for electrode placement.	39
Figure 12 – Operating room (OR) with synthetic brain phantom ready for electrode placement using the robotic system.	39
Figure 13 – Comparison between frame-based planned electrode trajectories (color lines) and those achieved after surgery (showed by the sliced view of the contacts in bright gray) using CT scan of a synthetic brain model in OR with stereotactic frame.	40
Figure 14 – Electrodes fixed to the synthetic brain phantom in OR with robotic system.	41

LIST OF ABBREVIATIONS AND ACRONYMS

SEEG - Stereoeletroencefalography

ROS - Robot Operating System

EP - Entry Point

EPE - Entry Point Error

TP - Target Point

TPE - Target Point Error

DBS - Deep Brain Stimulation

OR - Operating Room

mock-OR - Mock Operating Room

DBS - Deep Brain Stimulation

CT - Computed Tomography

MRI - Magnetic Resonance Imaging

FOV - Field of View

ROI - Region of Interest

ICP - Iterative Closest Point

DOF - Degrees of Freedom

GUI - Graphical User Interface

API - Application Programming Interface

PLA - Polylactic Acid

CONTENTS

1	INTRODUCTION	17
2	OBJECTIVES	19
3	LITERATURE REVIEW	21
3.1	Epilepsy	21
3.2	Treatment Methods	22
3.2.1	Video-EEG	22
3.2.2	Invasive EEG: Subdural EEG (SDE) and Stereoencephalography (SEEG)	23
3.3	Stereoelectroencephalography: Operation Methods	24
3.3.1	Stereotaxy	24
3.3.2	Frame-based Surgeries	24
3.3.3	Robot-based Surgeries	28
4	METHODS	31
4.1	Patient Monitoring	31
4.2	SEEG Planning Phase	31
4.2.1	Image Fusion	32
4.2.2	Electrode Placement	32
4.3	Robot-Scan Registration Phase	32
4.4	Intra-Operation Phase	33
5	METHOD AND RESULTS	35
5.1	Conical Target Phantom	35
5.2	Synthetic Brain Phantom	37
5.3	Synthetic Brain Phantom in Operating Room	40
6	DISCUSSION AND CONCLUSION	43
	REFERENCES	45

1 INTRODUCTION

In cranial neurosurgery, intracranial electrode placement is a core procedure for both diagnostic and therapeutic purposes, particularly in the management of epilepsy and movement disorders. These procedures require accurate insertion of electrodes into specific brain regions and are therefore increasingly assisted by robotic systems. Among the most common applications are stereoelectroencephalography (SEEG) for epilepsy diagnosis and deep brain stimulation (DBS) for treating movement disorders such as Parkinson's disease (KIM *et al.*, 2021).

SEEG involves the implantation of multiple depth electrodes into targeted brain areas to localize epileptogenic zones that are responsible for seizure generation. This technique provides critical information for surgical planning in drug-resistant epilepsy cases. In contrast, DBS is a therapeutic intervention where electrodes are implanted into subcortical structures, such as the subthalamic nucleus or globus pallidus, to deliver electrical stimulation that modulates abnormal neural circuits. DBS has become a standard treatment for movement disorders, notably Parkinson's disease, essential tremor, and dystonia, offering significant improvements in motor symptoms and quality of life for affected patients (LIU *et al.*, 2020).

Robotic systems are increasingly adopted for intracranial electrode implantation because they provide high accuracy and improve surgical workflow. Neuromate, introduced in the late 1990s, was among the first dedicated robotic platforms for neurosurgery, enabling automated and precise placement of electrodes for procedures such as SEEG and DBS. The subsequent development of ROSA brought further advancements, expanding its applications to include spine surgery and other orthopedic interventions. In epilepsy surgery, robotic assistance has proven particularly valuable, offering accuracy in localizing and targeting epileptogenic zones comparable to traditional methods while significantly reducing operative time (KAEWBORISUTSAKUL *et al.*, 2024).

Although SEEG requires precise electrode placement, its accuracy requirements are generally less stringent than those for deep brain stimulation (DBS), which demands submillimeter precision due to the need for targeting specific anatomical nuclei. SEEG, in contrast, is hypothesis-driven and aims to sample broader brain regions based on clinical hypotheses rather than discrete anatomical targets (BONDA *et al.*, 2021).

SEEG represents a clinically relevant and technically feasible entry point for robotic intervention, given its procedural characteristics and the growing demand for minimally invasive, accurate, and efficient electrode implantation in epilepsy surgery. Accordingly, this work focuses on the evaluation of a collaborative robotic system designed for SEEG

electrode placement called *Yara*, as an initial and essential step toward advancing robotic assistance in intracranial procedures. To contextualize this objective, the following chapters review the clinical aspects of epilepsy (Sec. 3.1), the classification and impact of seizure types, and the current therapeutic strategies available (Sec. 3.2).

2 OBJECTIVES

The primary objective of this work is to evaluate the accuracy of the Yara collaborative robotic platform for intracranial electrode placement during SEEG (stereoelectroencephalography) procedures. This evaluation is performed using anatomical phantoms that closely mimic human cranial structures to measure electrode placement accuracy. By focusing on phantom-based experiments, the study aims to establish a baseline for the systems technical performance in a controlled environment prior to any clinical application.

A key objective is the design and fabrication of cranial phantoms specifically for SEEG accuracy validation. These phantoms are developed to replicate the anatomical and mechanical properties of the human skull and brain, allowing for reproducible assessment of electrode placement. The creation of these phantoms is essential to ensure that the experimental conditions closely simulate those encountered in actual surgical scenarios.

Finally, the study aims to conduct accuracy validation tests using the Yara robotic platform, both in the laboratory and in the operating room environment. By performing electrode placement trials in these settings, the work seeks to assess the systems performance under different conditions, identify potential sources of error, and provide quantitative data on placement accuracy.

3 LITERATURE REVIEW

3.1 Epilepsy

Epilepsy is a chronic brain disease characterized by a long-lasting predisposition to generate seizures, not caused by any immediate insult to the central nervous system, and by the neurobiological, cognitive, psychological, and social consequences of recurrent seizures (BEGHI, 2020). It is the most common neurological diseases worldwide, affecting different social classes, ages, and geographic locations (NGUGI *et al.*, 2010).

The definition of an epileptic seizure is a repeated and transient episode that manifests through patterned behaviors and reflects underlying neural processes associated with the condition (FISHER *et al.*, 2005). Although all people with epilepsy experience seizures, not all individuals with seizures have epilepsy. Epileptic seizures can also occur after an acute injury to the central nervous system (CNS) of structural, systemic, toxic, or metabolic origin; these events are considered acute manifestations of the insult and may not recur once the underlying cause has been removed or the acute phase has passed (BEGHI *et al.*, 2010).

Epileptic seizures are categorized according to three main characteristics: origin in the brain, state of consciousness during the seizure, and level of body movement. Seizures can be classified as focal or generalized based on the first characteristic. The second characteristic considers whether consciousness is intact or impaired during the seizure, while the third characteristic refers to body movement, which may present motor or non-motor reactions (BEGHI, 2020).

Motor seizures encompass a variety of distinct manifestations. Atonic crises are characterized by a sudden and temporary loss of muscle tone, resulting in a sudden fall of the individual. On the other hand, tonic crises involve a sudden and prolonged increase in muscle tone, leading to intense stiffness. Clonic seizures are marked by rhythmic and repetitive muscle contractions, which can affect different parts of the body, while myoclonic seizures are characterized by rapid and sudden muscle contractions that can involve a specific muscle group or the entire body. Epileptic spasms, automatisms, and hyperkinetic seizures are also categorized (SARMAST; ABDULLAHI; JAHAN, 2020).

On the other hand, non-motor crises can present different forms of manifestation. They can be autonomic, involving dysfunctions in the autonomic nervous system, such as changes in blood pressure or heart rate. In addition, there may be crises of behavioral arrest, during which the individual may appear paralyzed or unable to perform voluntary movements. Cognitive crises affect cognitive function and may include memory lapses or mental confusion. Emotional crises are related to changes in the emotional state, such as

feelings of fear, anxiety, or euphoria. Finally, sensory crises affect the senses and can cause abnormal sensations, such as visual or auditory hallucinations (SARMAST; ABDULLAHI; JAHAN, 2020).

3.2 Treatment Methods

Epilepsy affects an estimated 70 million people worldwide; about 40% of these patients experience drug-resistant seizures. In such cases, surgery may be considered as a therapeutic option. This procedure is indicated for patients with disabling focal epilepsy who are unresponsive to drug treatment and whose seizures originate in a specific region of the brain that can be removed with minimal risk of neurological or cognitive dysfunction (MILLER; HAKIMIAN, 2013). Surgery can significantly improve quality of life by providing better seizure control and reducing dependence on high-cost or potentially harmful antiepileptic medications.

Correctly locating the seizure focus is crucial when preparing for surgery in patients with epilepsy (MILLER; HAKIMIAN, 2013). Localization methods aim to determine the focal region accurately, minimizing surgical invasiveness while seeking complete removal of the epileptogenic zone.

This is especially important, as the removal of critical areas of the brain can result in functional deficits, such as impairment of speech, memory, motor coordination, among other functions, depending on the location of the focus. Therefore, ensuring accurate location of the focus is essential to guarantee good surgical results and minimize potential adverse effects.

3.2.1 Video-EEG

Before progressing to invasive procedures, a non-invasive analysis is typically performed to identify potential areas of seizure foci and to guide further investigation. Scalp EEG is the primary non-invasive technique used for this purpose. Electrodes are placed on the patient's scalp using a cap or similar device, enabling monitoring during interictal (between seizures), ictal (during seizures), and post-ictal (after seizures) periods. This superficial electrode arrangement measures electrical potentials generated by neuronal activity near the skull. Standard systems use 32, 64, or 96 electrodes distributed across the scalp, with higher-density arrays (up to 256 channels) available for more detailed studies (SUN; MOU, 2023). Scalp EEG is essential for initial diagnosis and localization of seizure activity, providing critical information before invasive methods are considered (MILLER; HAKIMIAN, 2013).

3.2.2 Invasive EEG: Subdural EEG (SDE) and Stereoencephalography (SEEG)

Subdural EEG (SDE), also known as electrocorticography (ECoG), was developed to provide more precise measurement of brain activity than scalp EEG. In SDE, an electrode array is placed directly on the surface of the cortex after a portion of the skull is removed, as illustrated in Fig. 1. This direct contact enables the acquisition of signals with higher fidelity and less noise compared to scalp EEG (LESSER; CRONE; WEBBER, 2010). The electrodes typically remain in place for several days to record both ictal and interictal activity. However, SDE is highly invasive, requiring two craniotomies, one for electrode placement and another for removal, and carries a significant risk of postoperative infection, often related to surgical contamination. These drawbacks have motivated the development of alternative methods, such as SEEG, which aim to reduce invasiveness and associated complications (JEHI *et al.*, 2021).

In France, in the 1950s, Jean Talairach and Jean Bancaud developed a method that monitors deep parts of the cortex through insertion of depth electrodes, seeking to replace SDE (MAZOYER, 2008). This method was called Stereoelectroencephalography (SEEG) and today it is one of the most adopted invasive methods for locating the focal zone of seizures. SEEG does not present many of the problems associated with SDE. In this method, cylindrical electrodes (more like small wires) are introduced through small holes in the skull, without the need for craniotomy. SEEG has lower rates of infection, hemorrhage, neurological deficits, and morbidity compared to SDE, in addition to being a faster procedure, allowing the analysis of deeper brain tissues and having shown greater effectiveness in localizing and controlling seizures after surgical treatment (FIANI *et al.*, 2021). Fig. 1 illustrates the positioning of electrodes in scalp EEG, Subdural EEG (electrocorticography), and SEEG.

Electrodes implanted during SEEG are used to properly identify the epileptogenic zone (EZ) (JONES *et al.*, 2018). Planning prior to surgery is carried out to define the number of electrodes, the position of the entry points, and the target point of each electrode. Metrics are defined for evaluating the position of the SEEG implants. Entry points are defined as the point at which the electrode initiates contact with the surface of the brain or the skull. Target points are defined as the final position of the electrode, usually in a region within the brain.

Widely adopted metrics for evaluating the accuracy of the electrode placement are the Euclidean distance between the planned entry points and the post-surgical entry points, and the distance between the planned target points and the post-surgical target points.

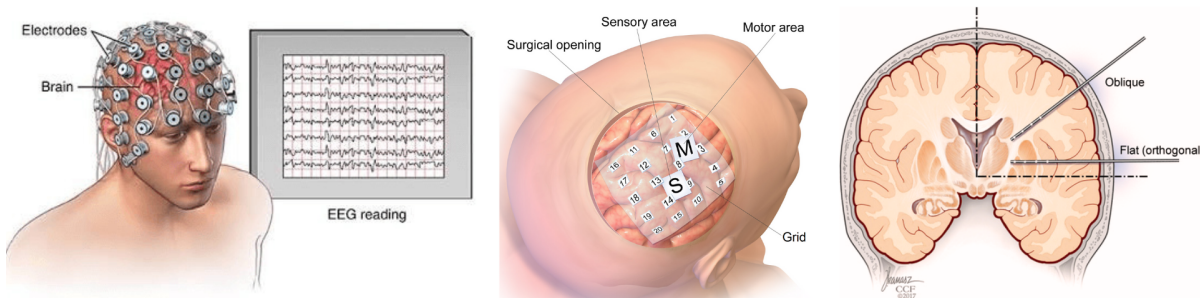


Figure 1 – Positioning of electrodes in scalp EEG, subdural EEG (SDE), and SEEG procedures respectively (SHEN, 2020) (Blausen.com staff, 2014) (JONES *et al.*, 2018).

3.3 Stereoelectroencephalography: Operation Methods

3.3.1 Stereotaxy

SEEG operation techniques began in the 1950s with Jean Talairach and Jean Bancaud, who developed x-ray based methods for planning and verifying electrode positioning. Since then the development of mechanical stereotactic apparatus to fix the skull and guide electrode placement concentrated in the mid 20th century (late 1940s-1950s). The early Talairach apparatus featured skull fixation pins, a support for the x-ray tube, and radiographic film (MAZOYER, 2008). Contemporary popular frames, such as the Leksell frame developed in Sweden around the same period, trace their origins to these innovations.

With the advent of computed tomography, surgeries began to be planned based on slices, allowing a three-dimensional understanding of the areas of investigation. Devices that use the three-dimensionality of tomography images were adapted, adding a support with a diagonal cut in the shape of an N, allowing the calculation of the height of each tomography slice in relation to the device coordinates. This system became known as the N-Localizer and is widely used in current neurosurgeries (LOZANO *et al.*, 2009).

3.3.2 Frame-based Surgeries

The earliest SEEG technique involved introducing electrodes in parallel trajectories, normal to the sagittal view, using the Cartesian map called Talairach coordinates

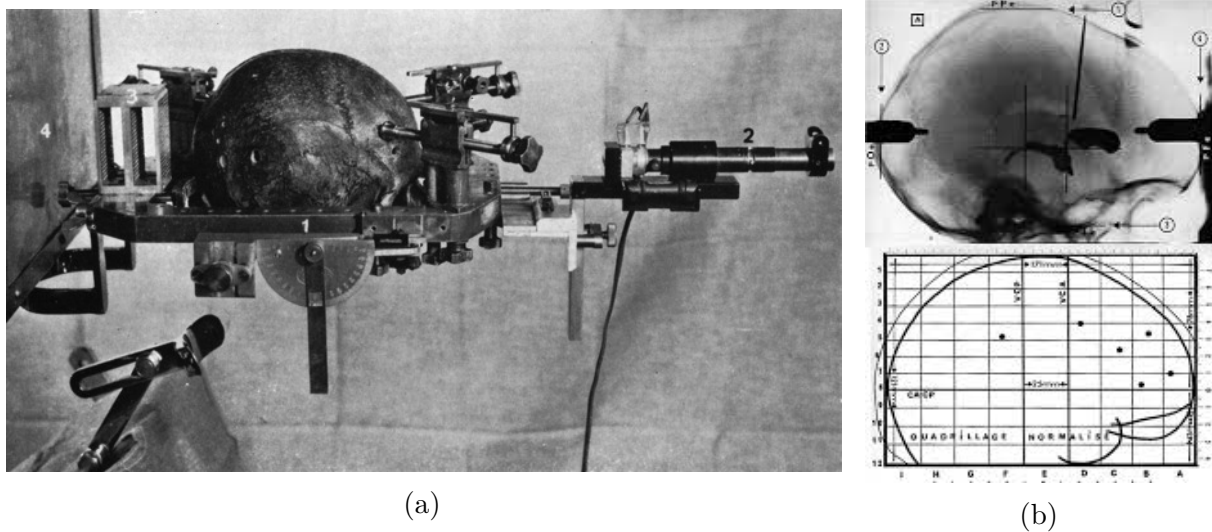


Figure 2 – (a) presents Talairach's frame with x-ray supports and (b) presents an example x-ray image alongside the coordinate system developed by Talairach (MAZOYER, 2008).

(MAZOYER, 2008). Subsequently, variations of the technique were explored with the introduction of stereotactic arcs that can be fixed to devices such as the Leksell or CRW and that allow the introduction of oblique electrodes. Therefore, the assessment of the impact on precision between different techniques for implanting oblique or orthogonal electrodes was studied in (IORDANOU *et al.*, 2019). Figure 3 presents the Leksell G apparatus and the N-Localizer.

Originally, the calculation of the coordinates of each electrode in relation to the apparatus was carried out manually, using the N-Localizer geometry. Some surgical planning software automated the calculation of entry and target coordinates using image-processing methods that detect the N-Localizer (DASGUPTA *et al.*, 2022). These programs also feature planning tools such as fusion of CT and MRI images.



Figure 3 – Frame Leksell G without N-Localizer and with N-Localizer respectively (ROJAS-VILLABONA *et al.*, 2016).

Image fusion allows precise surgical planning by combining preoperative MRI to

assess vascular structures and functional anatomy near electrode trajectories and intraoperative CT to permit frame positioning. During surgery, a stereotactic frame and N-Localizer are attached to the patient's head, followed by an intraoperative CT scan. This scan is fused with the preoperative MRI, enabling the planning software to identify N-Localizer fiducials and accurately compute coordinates for electrode placement. These coordinates are then inputted into the stereotactic frame or arc, guiding the surgeon in positioning each electrode along the planned trajectory.

Surgeries based on stereotactic devices have a broad history of use, but they also have disadvantages relative to more recent systems, such as robotic platforms. Among the disadvantages, stereotactic frame-based procedures require placement of the apparatus at the beginning of surgery, followed by an intraoperative CT generally performed in another room, and the fusion of this CT with the MRI used for planning. This intraoperative CT is not necessary with frameless robotic systems.

The Table 1 presents a comparison between the procedures necessary to perform frame-based surgery compared to frameless surgeries. The greater number of steps during surgery increases the time needed to perform the surgery and may result in loss of accuracy due to non-deterministic procedures and possible human errors.

Performing a CT scan during surgery is time-consuming. The frame-based process requires a tomography with the stereotactic device immediately after its placement. While having a CT scanner available in the same operating room would streamline logistics, this setup is rarely feasible, as most hospitals do not have a dedicated CT scanner for each operating room. Although some facilities offer operating rooms equipped with CT scanners, their limited availability and competition with other ongoing surgeries complicate scheduling and scalability. As a result, the typical solution is to transport the sedated patient to a separate CT scanner, which increases surgery time and possibly introduces additional risks.

Another significant source of error arises from the fusion of intraoperative CT images acquired with the stereotactic device and preoperative MRI images. Image fusion involves the precise alignment of two volumetric datasets - typically, the CT and MRI scans - so that both accurately represent the same anatomical structures. This process is necessary because the spatial orientation and coordinate systems of the CT and MRI volumes differ in space due to variations in patient positioning and scanner-specific parameters. Imperfect alignment during fusion can introduce discrepancies in the localization of entry and target points, thereby contributing to the overall error in electrode placement.

The alignment of the preoperative MRI with the intraoperative CT, in the case of SEEG surgery, allows the planning performed on the MRI to be accurately transferred to the CT acquired with the stereotactic apparatus. In this way, the result of the fusion is the planning of the surgery, containing entry and target points in the same reference as

Table 1 – Comparison between frame-based and *frameless* procedures for SEEG.

Frame-based surgery

1. Preoperative imaging (MRI, EEG) and clinical evaluation
2. Trajectory planning based on preliminary evidence before surgery
3. Start of surgery and fixation of the head in the stereotactic apparatus
4. Tomography with stereotactic frame and N-Localizer
5. Fusion of MRI and intraop CT with frame to calculate the coordinates of each electrode in relation to the apparatus
6. Using the stereotactic ruler, drill the skin and skull using a 3 mm drill with an appropriate end point
7. Fixing a guide screw to the skull, to serve as a guide for electrode insertion
8. Using the guide screw, insert the temporary stylet into the intracranial space to the target point for electrode guidance
9. Remove the temporary stylet and, through the guide screw, insert the depth electrode into the intracranial space to the predefined destination
10. Screw the electrode cover onto the guide screw
11. Repeat steps 6 to 10 for the remaining electrodes

Robot-assisted frameless surgery

1. MRI, EEG, and preliminary surgery exams, as well as assessment of patient symptoms
2. Planning trajectories based on preliminary evidence before surgery using the robot's interface
3. Facial registration using fiducial points of the face
4. Positioning the robot and drilling the skin and skull using a 3 mm drill with an appropriate limit stroke
5. Fixing the guide screw to the skull
6. Using the guide screw, insert the temporary stylet into the intracranial space to the target point for electrode guidance
7. Remove the temporary stylet and, through the guide screw, insert the depth electrode into the intracranial space to the predefined destination
8. Screw the electrode cover onto the guide screw
9. Repeat steps 4 to 8 for the remaining electrodes

the apparatus images, thus allowing the calculation of the coordinates necessary to align the ruler or stereotactic arc in each trajectory. Even in the most ideal case, this process is not perfect and will contribute to the final error of each trajectory.

In summary, the introduction of frame-based stereotactic techniques advanced numerous procedures and contributed to the development of novel surgical methods, establishing them for many years as the gold standard. Nevertheless, the operational workflow required by frame-based systems presents several disadvantages. Frame fixation, patient transport to the CT, and the image-fusion process increase operative time and procedural complexity, and may contribute to the cumulative error affecting each trajectory in SEEG.



Figure 4 – Robots capable of performing SEEG surgeries: Zimmer Biomet ROSA ONE Brain, Brainlab Cirq and Renishaw Neuromate respectively.

3.3.3 Robot-based Surgeries

The frame limitations motivated the development and adoption of frameless robotic systems for SEEG surgeries. Neuromate, introduced in the late 1990s, was among the first commercially available robots for SEEG neurosurgery (CARDINALE FRANCESCO MD *et al.*, 2013). Subsequently, Medtech (acquired by Zimmer Biomet) developed ROSA ONE Brain in 2007, and Brainlab introduced Cirq, both capable of performing SEEG procedures. These systems also support other neurosurgical interventions, including brain biopsies and DBS. Figure 4 shows Neuromate system, which features a triangular base fixed to the floor and supports for skull fixation using Mayfield or Leksell frames.

A large series reporting on a total of 500 procedures established the safety and accuracy of Stereoelectroencephalography (SEEG) methodology, confirming a low major complication rate of 2.4%, and demonstrating a median target point localization error of 1.77 mm for the modern robot-assisted workflow (CARDINALE FRANCESCO MD *et al.*, 2013). Building on this foundation, subsequent prospective series, such as one of 100 patients (101 procedures, 1245 electrodes), demonstrated that robot-assisted SEEG is safe, accurate (median EPE 1.2 mm, TPE 1.7 mm), and efficient (planning 30 min, operative 130 min), yielding seizure freedom in 66% of resected patients with a 4% complication rate, and showing comparable accuracy with shorter operative times than traditional frame-based methods (GONZALEZ-MARTINEZ *et al.*, 2016).

Current robotic SEEG systems, while beneficial, have room for significant improvement. Some reports show that adoption of the Neuromate platform has been constrained by limitations in allowable patient positioning, which restrict its compatibility with some intraoperative workflows (KAJITA *et al.*, 2015). In addition, the system's limited portability requires allocation of a dedicated operating room, creating a logistical barrier to clinical deployment. The robot is a 5DOF manipulator, presenting reduced range of possible end-effector (EF) poses compared with conventional 6DOF robots, thereby limiting trajectory flexibility for certain electrode insertions.

ROSA lacks many collaborative-arm features. Although designed to work alongside

the surgeon, it does not include sensors common to collaborative systems, such as joint-torque sensing and automatic collision detection and braking. For this reason, ROSA operates as a conventional robot in collaborative tasks, placing the surgeon and patient at higher risk than with true collaborative systems. Yara, the system proposed in this project, uses collaborative robots designed for shared operation with humans, enhancing the safety of both surgeon and patient.

This project presents the accuracy of Yara, a collaborative robotic platform developed for frameless intracranial electrode placement procedures, designed to offer accuracy, reduced surgical time, and enhanced safety compared to traditional frame-based methods. The system integrates planning software for defining electrode entry and target points, MRI/CT image fusion, automated patient registration using depth cameras, and collision-free robotic positioning. In this work, we present a comprehensive evaluation of the accuracy of the Yara platform for SEEG electrode placement, based on phantom experiments that simulate clinical conditions.

4 METHODS

This chapter presents the workflow and methodology underlying the use of the Yara robotic system for SEEG surgery. It begins with patient monitoring and data acquisition (Sec. 4.1), then describes the planning phase, including image fusion and electrode placement (Sec. 4.2). The subsequent robot-scan registration phase (Sec. 4.3) addresses the alignment of preoperative imaging with the robotic system. The intraoperative phase (Sec. 4.4) outlines the integration of robotic assistance for electrode insertion. The chapter concludes with the methods and results of system accuracy evaluation and validation (Sec. 5).

4.1 Patient Monitoring

Patient monitoring for SEEG candidates involves comprehensive video-EEG and MRI assessments to localize epileptogenic zones and determine surgical eligibility, as detailed in Sec. 3.2.1. Once a focal epilepsy amenable to surgical intervention is identified, and SEEG is selected as the preferred invasive technique, the workflow proceeds to the planning phase, where the robotic system assists in precise electrode trajectory definition.

4.2 SEEG Planning Phase

The user interface is prepared for SEEG planning, developed to address neurosurgeons' and neurologists' needs during planning. The goal of planning is to select target points so that the electrodes cross the most probable epileptogenic zone. Entry points need to be selected so that the electrode trajectory is safe and follows a path without collision with critical structures such as arteries or eloquent regions of the brain. Typically, electrodes have between 5 and 15 contacts along their length, spaced a couple of millimeters apart. Between 5 and 10 electrodes are typically placed during an SEEG procedure.

For SEEG planning, the surgeon requires MRI images to visualize soft tissues, brain structures, and vascularization, as well as CT images that provide precise information about the skull. Combining these modalities through image fusion enables the simultaneous assessment of critical anatomical features, such as blood vessels, gray and white matter, and bone structures in a unified reference frame. This alignment is essential for safe and effective electrode placement, as it allows the surgeon to avoid critical regions and optimize the trajectory of each electrode.

4.2.1 Image Fusion

For image fusion, we adopted the method described in (KLEIN *et al.*, 2009), which enables the alignment of CT-CT, MRI-MRI, or CT-MRI images. The fusion process aims to optimize the mutual information metric, identifying the transformation that best aligns a source image with a target image. In multimodal fusion scenarios such as CT-MRI, the images differ in tissue representation and contrast (bone appears bright in CT but is nearly invisible in MRI). Mutual information serves as a statistical measure of the shared information between two random variables. In image registration, it quantifies how well one image explains the other, independent of intensity values, making it effective for multimodal image alignment.

4.2.2 Electrode Placement

After analyzing the images, electrode trajectories are planned by determining the entry and target points and specifying electrode parameters such as contact spacing, coordinates, number of contacts, and physical dimensions. This step is performed a couple of days before surgery; the planned electrodes are saved and loaded into the interface on the day of surgery. Small adjustments can be made during the operation if needed.

4.3 Robot-Scan Registration Phase

Before starting the operation, it is essential to perform a registration procedure to align the coordinate systems of the preoperative scans and the robot. This step ensures that the positions of the planned electrode trajectories correspond accurately to the physical space in which the robot operates. The registration method adopted in this work is known as fiducial registration, which involves identifying and matching a set of anatomical or artificial landmarks (fiducials) in both the image space and the physical space. By determining the transformation that best aligns these corresponding fiducial points, the system can accurately map planned positions from the imaging data to the robot's coordinate system (ZENG *et al.*, 2017). This alignment is fundamental for transferring surgical plans to the robotic system and ensuring precise execution during the procedure.

The procedure begins by identifying several fixed anatomical or artificial landmarks, known as fiducial points, within the preoperative images. These same points are then physically located on the patient using the robotic arm. To record each corresponding point, the operator positions the robot's tool at the desired location and confirms the selection. The collected coordinates are transmitted to the robot's control module, which computes the optimal rigid transformation using the ICP method.

Expanding on the ICP method by (GAO *et al.*, 2017), the goal is to find the matrix \mathbf{R} and vector \mathbf{t} that best solve the Euclidean transformation 4.1 given a matched set of 3D points such as $\mathbf{P} = \{\mathbf{p}_1, \dots, \mathbf{p}_n\}$ and $\mathbf{P}' = \{\mathbf{p}'_1, \dots, \mathbf{p}'_n\}$.

$$\forall i, \mathbf{p}_i = \mathbf{R}\mathbf{p}'_i + \mathbf{t} \quad (4.1)$$

In this procedure, fiducial landmarks are selected that are anatomically distinct and reproducible points on the patient's head, reliably identifiable both in the CT/MR images and in physical space. Commonly used fiducials include the nasion (the indentation between the forehead and the nose), the left and right preauricular points (just in front of each ear), and sometimes additional points such as the tip of the nose or the outer canthi. These landmarks are chosen for their ease of identification and for exhibiting minimal movement relative to the skull, avoiding softtissue deformation.

The system computes the transformation ${}^{robot}T_{scan}$ that best aligns the two sets of points, minimizing the reprojection error and ensuring that the planned trajectories in the image space correspond precisely to the patient's anatomy in the real world. The reprojection error is computed by transforming the fiducial points in the scan space (${}^{scan}P_{virtual}$) to the robot space and comparing them with the collected fiducials (${}^{robot}P_{real}$) in the target space (Equation 4.2).

$$Reproj = ||{}^{robot}P_{real} - {}^{robot}T_{scan} {}^{scan}P_{virtual}|| \quad (4.2)$$

4.4 Intra-Operation Phase

The next step is the surgery for the precise placement of electrodes in the patient. The system incorporates a digital twin of the robot within its interface, providing real-time visualization of the robots position and planned movements. Before executing any planned motion, the system displays the intended trajectory and requires explicit confirmation from the operator. This workflow ensures that each step of the surgical process is performed with maximum safety and situational awareness.

During the trepanation process, the system assists the surgeon by displaying the precise drilling depth required to safely penetrate the skull without breaching the dura mater. Once the bone has been traversed, a drill guide is positioned to maintain the correct trajectory and stabilize the electrode. The interface then provides the exact insertion depth needed for the electrode to reach the planned intracerebral target, ensuring accurate and safe placement.

5 EXPERIMENTS AND RESULTS

As discussed in Sec. 3.3, an SEEG method must be sufficiently accurate to place each electrode at the planned position and orientation. The accuracy can be measured by the Euclidean distance between the planned entry point and the entry point achieved after the surgery. The same method applies to the target point. The angle between the entry-to-target vector $\vec{P_{target}} - \vec{P_{entry}}$ for the planned electrodes and the postoperative electrodes reflects the orientation error.

To comprehensively assess the accuracy of the Yara system for SEEG surgeries, we developed and tested three distinct phantom models, each with a dedicated evaluation setup: (1) a conical target phantom in a mock-OR, (2) a synthetic brain phantom in a mock-OR, and (3) a synthetic brain model assessed under actual OR conditions.

The experiments were conducted in a controlled laboratory environment designed to closely mimic the conditions of an actual operating room. This setup included a surgical table, a head clamp for securing the phantom or synthetic head, and the complete robotic system mounted on its dedicated cart. The laboratory environment allowed for iterative testing and refinement of the workflow, ensuring that all components of the system functioned as intended before transitioning to a clinical setting.

Following laboratory assessments, the system was evaluated in the OR at the Hospital das Clínicas da Faculdade de Medicina de Ribeirão Preto (HC-FMRP-USP). In this environment, the robot and its cart were transported and installed according to standard OR protocols. The tests in the OR aimed to assess the system's performance under actual clinical conditions, including the presence of medical staff and integration with existing surgical infrastructure.

5.1 Conical Target Phantom

To validate the system's accuracy using a phantom, we employed a 3D-printed phantom of a child's head, along with a base containing cylinders topped with cones. The patient data used for the phantom model was approved for research use, and no personal or identifiable information is available. The apex of each cone served as a target point, requiring the system to position a thin metal rod, simulating an electrode, precisely at these locations. During the planning phase, entry points were arbitrarily distributed across the skull surface to maximize variability, while target points corresponded to the cone peaks. Registration was performed using fiducial markers placed on the head surface, following the same protocol as the synthetic brain validation.

During the operation phase, the robot sequentially positioned itself at each planned

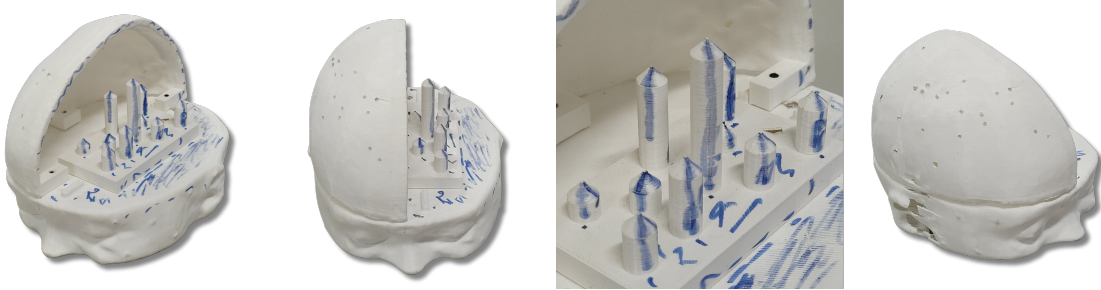


Figure 5 – Conical targets phantom used for quantitative accuracy assessment via stereoscopic imaging.

electrode site. The interface provided the required drilling depth, guiding the placement of the drill stop, and calculated the insertion length needed for the rod to reach the target point.

To measure the accuracy of the system, we utilized a stereo camera setup to capture images of the phantom after rod insertion. The stereo camera allowed for precise measurement of the distance between the tip of the inserted rod and the apex of each cone, representing the planned target point.



Figure 6 – Conical targets phantom in SE for metal rods positioning using the robotic system.

The stereo image pair was acquired using a rectified stereo camera with a 4 cm baseline and a resolution of 1920×1080 pixels, with known intrinsic parameters. The tip of the rod and the cone apex were manually marked in both images, with an average marking error proportional to depth. We assumed a linear disparity pixel error ranging from 0 to 5 pixels for depths from 0 to 2.5 meters. The depth error was calculated using Formula 5.1, where z is the depth, e_{disp} is the disparity error in pixels, b is the distance between the cameras in meters, and f is the focal length in pixels. The derivation of Eq. 5.1 is shown in Eq. 5.2.

$$\delta z = \frac{z^2 e_{\text{disp}}}{fb + e_{\text{disp}} z} \quad (5.1)$$

$$z = \frac{fb}{d} \Rightarrow \delta z = z - z' = \frac{fb}{d} - \frac{fb}{d + e_{\text{disp}}} = \frac{fbe_{\text{disp}}}{d(d + e_{\text{disp}})} = \frac{z^2 e_{\text{disp}}}{fb + e_{\text{disp}} z} \quad (5.2)$$

Electrode	1	2	3	4	5	6	7	8	9	Mean
Δ Target (mm)	1.5	1.3	2.7	1.6	2.5	2.3	1.1	1.9	1.4	1.8 ± 0.3

Table 2 – Error in the positioning of target points planned and reached after surgery using a model with phantom and stereo camera to measure distances.

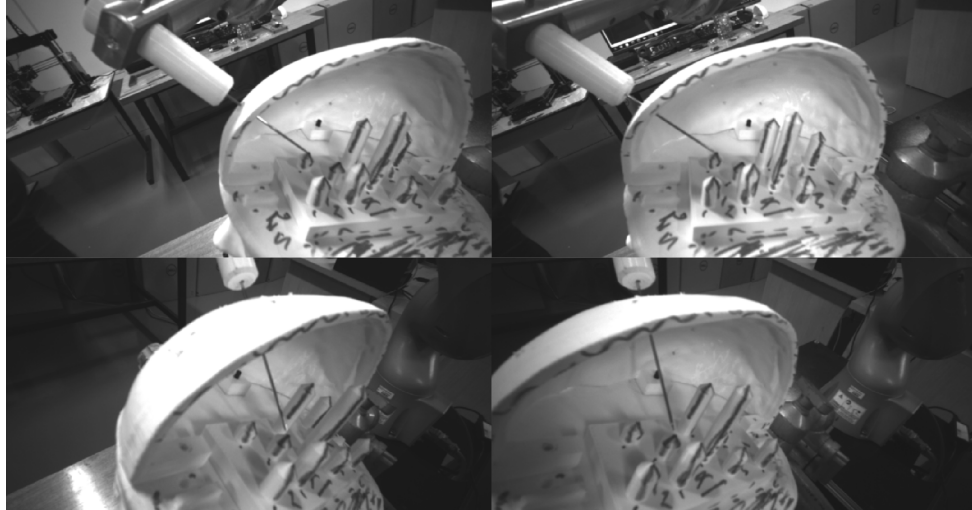


Figure 7 – Examples of stereo camera images used to measure the distance between the metal rod tip and the planned target point. The top and bottom rows show the left and right images of a stereo pair for the same moment in time.

Using Eq. 5.1, it was possible to estimate a maximum measurement error of 0.3 mm, which corresponds to the largest expected uncertainty in the distance calculation due to stereo camera disparity error. Nine electrodes were inserted, followed by the target error estimation process. Fig. 6 presents the phantom and Fig. 7 presents images from the stereo camera used to calculate the error. Table 2 presents the target error for each electrode, resulting in an average error of 1.8 ± 0.3 mm.

5.2 Synthetic Brain Phantom



Figure 8 – Phantom model with synthetic brain produced using silicone rubber and 3D printed plastic surface skin after electrode placement.

To further evaluate the system, tests were conducted using a synthetic brain phantom. The phantom was created by molding the right hemisphere of the brain from silicone rubber to closely mimic the anatomical structure and consistency of real brain tissue. A

3D-printed head model was used to replicate the patient's head surface, including a section of the skull. This setup allowed for a realistic simulation of the SEEG procedure, enabling the robotic system to perform electrode placement in a controlled environment.



Figure 9 – Synthetic brain phantom in mock-OR during electrode placement with the robotic system. The rightmost image displays the postoperative CT scan of inserted electrodes.

A 3D-printed positive model of the brain was produced from patient imaging data. This positive was used to create a negative mold using silicone rubber. Once cured, the negative mold was filled with silicone rubber of Shore A 5 hardness, chosen to approximate the mechanical properties of brain tissue. To facilitate demolding, a release agent was applied to the mold surface. The resulting synthetic brain was then positioned inside the 3D-printed head model, which incorporated a section of the skull to closely replicate the patient anatomy (Figure 8).

Preoperative CT scan and a surgical plan were used to replicate the clinical scenario in a controlled laboratory environment. The robotic system was then employed to insert nine electrodes according to the planned trajectories. The procedure was completed successfully, demonstrating the system's ability to perform electrode placement in a surgical simulation. After the operation, the phantom with the electrodes placed invasively was taken for CT imaging to acquire images showing the internal positions of the electrodes. This allowed comparison between the inserted electrode positions and the surgical plan to calculate the system error.

Figure 8 shows the synthetic model developed. The comparison between the planned and achieved electrodes with the fusion of the postoperative CT with the preoperative images (Fig. 10) allows the calculation of Euclidean distances between the planned and achieved trajectories and, therefore, allows the evaluation of the system's accuracy (Table 3). The CT volume has an isotropic voxel spacing of 0.25 mm in all three dimensions, which was used as the measurement error.

Some limitations were observed during the tests, particularly regarding the adhesion between the electrodes and the silicone rubber material. This adhesion increased friction and made electrode insertion more difficult compared to real brain tissue, where such resistance is not typically encountered. As a result, the insertion process in the phan-

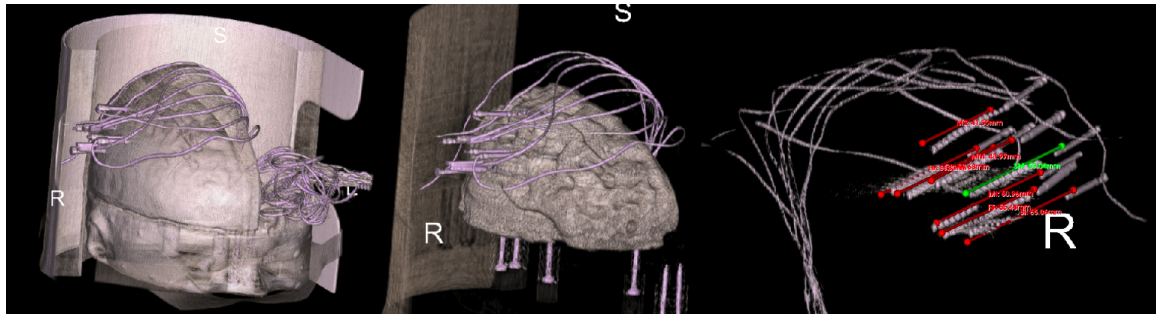


Figure 10 – Comparison between preoperative (red and green lines) and postoperative (gray contacts) electrode trajectories using CT scan of the synthetic brain model in the mock-OR.

Electrode	1	2	3	4	5	6	7	Mean
ΔEntry (mm)	1.47	1.81	1.58	1.71	0.56	0.95	1.04	1.30 ± 0.25
ΔTarget (mm)	2.57	2.62	3.72	2.26	4.88	3.48	1.97	3.07 ± 0.25

Table 3 – Error in positioning the entry and target points planned and reached after surgery using a synthetic brain model.

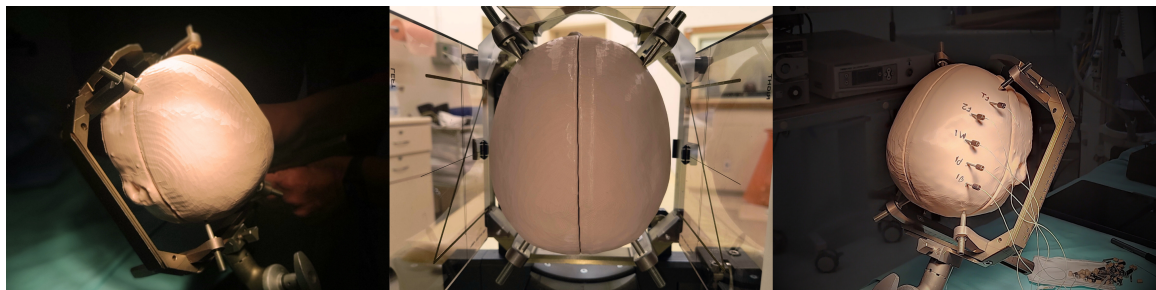


Figure 11 – Phantom model with synthetic brain placed in the OR using stereotactic frame for electrode placement.

tom did not fully replicate the ease of electrode placement observed in clinical practice. Nevertheless, the synthetic brain phantom provided a valuable platform for simulating electrode placement and quantitatively assessing system accuracy under controlled conditions.

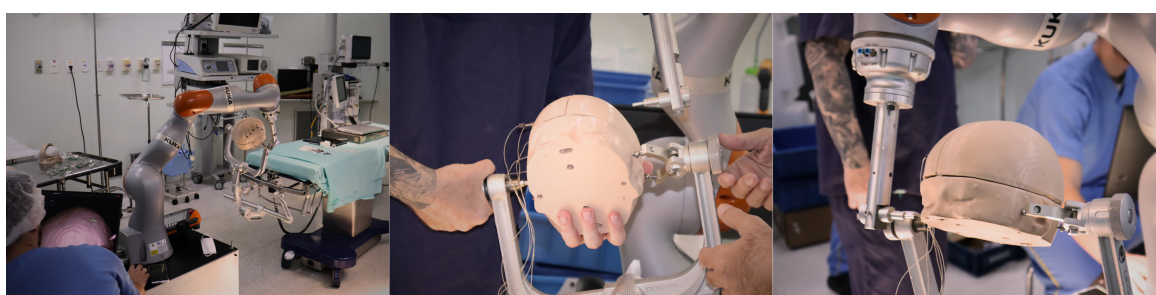


Figure 12 – Operating room (OR) with synthetic brain phantom ready for electrode placement using the robotic system.

5.3 Synthetic Brain Phantom in Operating Room

In order to evaluate the system in a real surgical environment, a second synthetic brain model was created. For this phantom, we produced a brain made of alginate to better simulate the consistency of real brain tissue. The surface of the head was again 3D printed to replicate the anatomical structure. The phantom was taken to the operating room, where the robotic system was used to perform electrode placement under actual surgical conditions, including the presence of medical staff and adherence to operating room protocols.

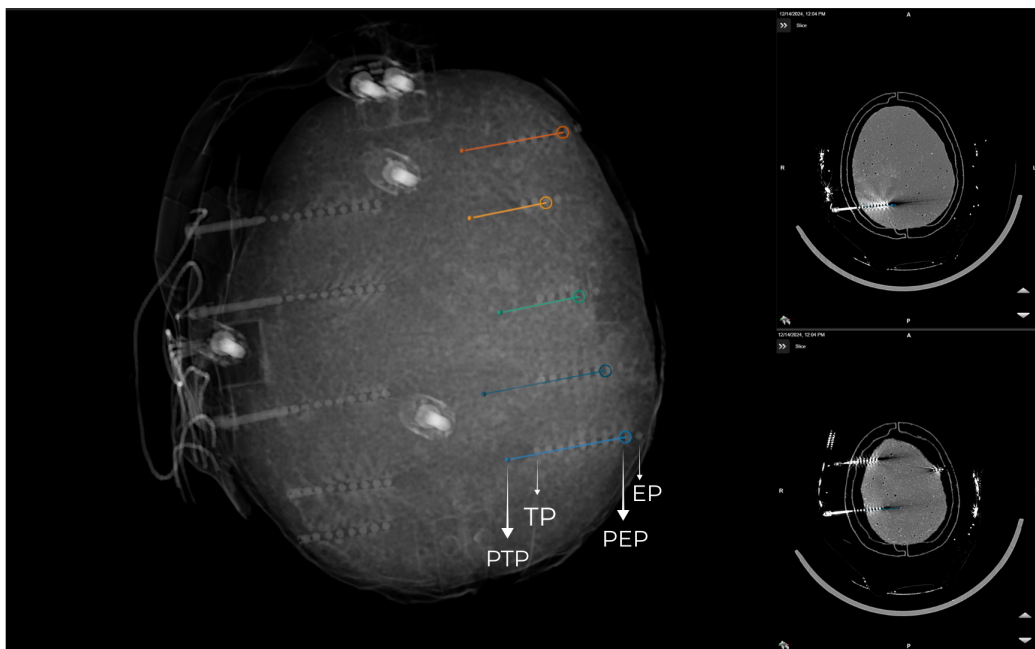


Figure 13 – Comparison between frame-based planned electrode trajectories (color lines) and those achieved after surgery (showed by the sliced view of the contacts in bright gray) using CT scan of a synthetic brain model in OR with stereotactic frame.

In the right brain hemisphere, we introduced the electrodes using stereotactic frame guidance, while in the left hemisphere, the procedure was performed using the robotic system. This approach allowed for a direct comparison between the traditional frame-based method and the robotic-assisted technique within the same surgical setting. After the procedure, a CT scan was performed to visualize the internal positioning of the electrodes. The postoperative CT images were then fused with the preoperative planning images to assess the accuracy of electrode placement.

For the stereotactic frame procedure, electrode trajectories were planned using preoperative MRI images. In the operating room, the stereotactic frame was securely attached to the phantom's head with the N-Localizer (see Sec. 3.3.2) and the assembly was transported to the CT scanner for image acquisition. The acquired CT images were fused with the preoperative MRI, enabling precise calculation of electrode coordinates within the

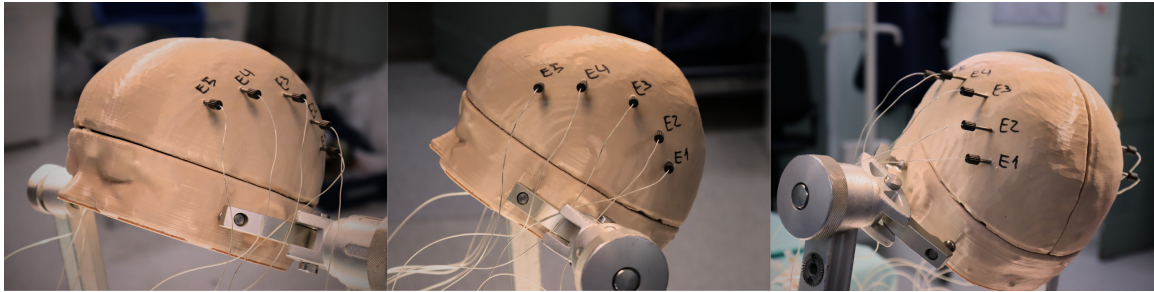


Figure 14 – Electrodes fixed to the synthetic brain phantom in OR with robotic system.

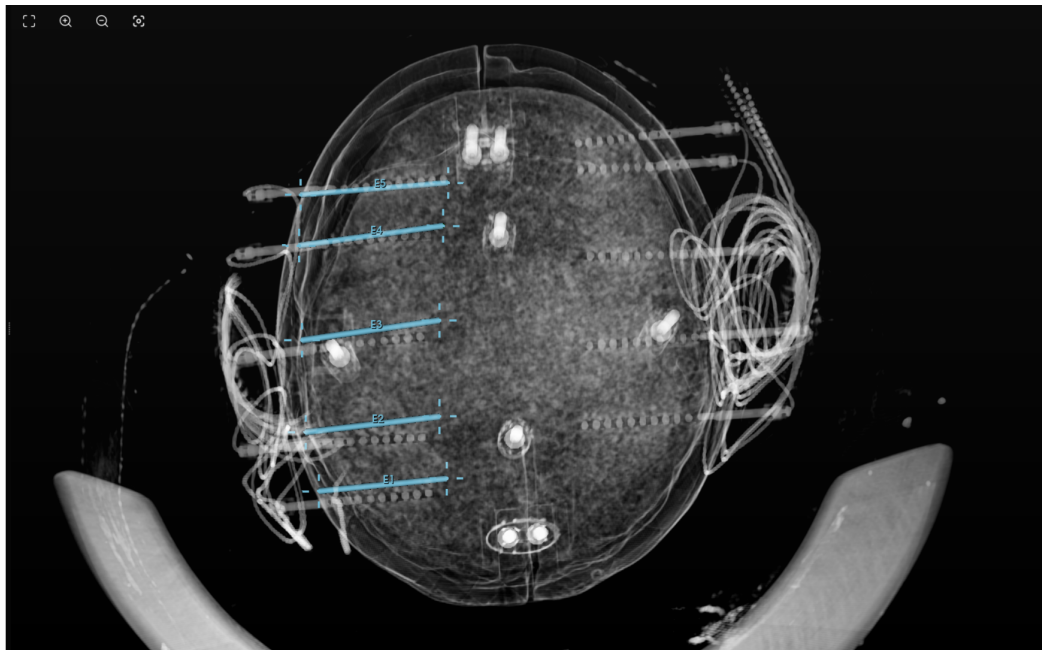


Figure 15 – Comparison between planned electrode trajectories (blue lines) and those achieved after surgery (3D contacts in gray) using CT scan of a synthetic brain model in OR with robotic system.

frame's coordinate system. Electrode insertion was then performed sequentially, guided by the stereotactic apparatus (Fig. 11). Finally, a postoperative CT scan was conducted to verify the actual positions of the electrodes (Fig. 13), fused with the preoperative images, and entry and target errors were calculated (Tab. 4).

Electrode	1	2	3	4	5	Mean
ΔEntry (mm)	1.6	2.1	1.8	3.6	5.0	2.8 ± 0.25
ΔTarget (mm)	8.1	16.2	11.1	15.3	13.9	12.9 ± 0.25

Table 4 – Error in positioning the entry and target points planned and reached after surgery using a synthetic brain model in the OR with stereotactic frame.

For the robotic procedure, the same preoperative MRI images served as the basis for planning. The phantom was stabilized in the Mayfield head clamp, and anatomical fiducial markers were collected using the robot for registration (Fig. 12). The robot autonomously positioned itself at each planned electrode site, and electrodes were inserted

along the pre-planned trajectories (Fig. 14). Unlike the frame-based approach, no intraoperative CT scan was required, as registration was accomplished directly using the anatomical fiducial markers.

Electrode	1	2	3	4	5	Mean
Δ Entry (mm)	3.1	3.7	2.9	3.2	2.6	3.1 ± 0.25
Δ Target (mm)	5.8	5.9	5.8	5.9	5.5	5.8 ± 0.25

Table 5 – Error in positioning the entry and target points planned and reached after surgery using a synthetic brain model in the OR with robotic system.

As in the frame-based procedure, postoperative CT images were fused with pre-operative MRI to evaluate electrode placement accuracy. Entry and target errors were calculated by comparing planned and actual electrode positions (Fig. 15, Tab. 5).

6 DISCUSSION AND CONCLUSION

The literature indicates that frame-based SEEG procedures can achieve a maximum entry point error (EPE) of 7.1 mm and target point error (TPE) of 8.5 mm, as documented in (GIRGIS *et al.*, 2020). Some studies have observed lower average errors, with EPE values of 1.51 mm and TPE values of 1.59 mm, which may be related to variations in surgical technique, image fusion accuracy, or other procedural factors. Robotic-assisted SEEG procedures have demonstrated comparable accuracy, with reported EPE and TPE values of 1.38 mm and 1.54 mm, respectively (ZHENG *et al.*, 2021). The meta-analysis presented in (VASCONCELLOS *et al.*, 2023) compared four robots, showing slightly greater TPE for ROSA and Neuromate than for other systems. In terms of operative duration, robotic-assisted surgeries have been shown to be more efficient, with an average time of 127 minutes compared to 152 minutes for frame-based methods (ZHENG *et al.*, 2021).

Regarding this study, the conical target phantom focused on evaluating the target error caused by intrinsic sources. These sources are defined as the internal aspects of the systems that can generate inaccuracies, such as the robot's kinematics, the EF tool tolerances, movements of the robot cart and vibrations, and the registration method. Since no electrode insertion was performed, errors related to the surgical procedure, such as brain shift and electrode bending, were not present in the results. The phantom tests resulted in an average TPE of 1.8 mm, which is comparable to the values reported in the literature for robotic-assisted SEEG procedures.

The synthetic brain phantom test was designed to assess the overall system accuracy by incorporating both intrinsic and extrinsic sources of error in a controlled environment. Extrinsic factors include procedural elements such as electrode bending, manual depth measurement inaccuracies, and interactions between the electrode and the synthetic brain material. The results indicated an average EPE of 1.3 mm and a TPE of 3.1 mm. While the EPE is consistent with values reported for robotic-assisted SEEG procedures in the literature, the slightly elevated TPE may be attributed to these additional extrinsic factors, particularly the friction and adherence between the electrode and the synthetic brain, which could have contributed to deviations during insertion.

The frame-based errors observed in this study (Sec. 5.3) were higher than in other studies (ZHENG *et al.*, 2021), primarily attributed to inaccuracies in the depth dimension. These discrepancies may be related to the properties of the synthetic brain model made of alginate, which may not perfectly replicate the mechanical properties and consistency of real brain tissue. Additionally, a systematic error may have been introduced during the manual calculation of the insertion depth, further contributing to the deviation between planned and achieved electrode positions. Since the focus of this work was not on the

frame-based method, a detailed analysis of these deviations was not conducted.

The simulation of the robotic-assisted method using the synthetic brain in the OR (Sec. 5.3) resulted in an average EPE of 3.1 mm and a TPE of 5.8 mm, which were higher than those observed in previous phantom experiments. This increase is likely due to additional extrinsic factors present in the OR environment. Notably, the Mayfield head clamp used in this setting was longer than the one employed in earlier tests, causing the structure to bend more during skull drilling. This increased bending contributed to higher EPE values, altered the entry angle, and consequently affected the TPE. To minimize this source of error, future designs could incorporate a more rigid and stable connection between the robot base and the patient’s head.

	Mock-OR		OR	
Method	Robotic	Robotic	Robotic	Frame-based
Phantom	Conical	Synthetic	Synthetic	Synthetic
EPE (mm)	-	1.3 ± 0.3	3.1 ± 0.3	2.8 ± 0.3
TPE (mm)	1.8 ± 0.3	3.1 ± 0.3	5.8 ± 0.3	12.9 ± 0.3

Table 6 – Accuracy summary for SEEG across environments, methods, and phantom types.

As highlighted in (ZHENG *et al.*, 2021), SEEG procedures are fundamentally hypothesis-driven: specific brain regions are targeted for electrode implantation based on preoperative evaluations, such as seizure semiology, imaging, and EEG findings, rather than on fixed anatomical coordinates as in deep brain stimulation (DBS). Electrode trajectories are therefore planned to test hypotheses about the origin and propagation of epileptic activity. Each SEEG electrode typically has a contact surface area of approximately 10 mm^2 , allowing it to record electrical activity from a large population of nearby neurons, and (DESSERT; THIO; GRILL, 2023) simulated that SEEG contacts can detect epileptiform signals up to 1.5 cm away. Consequently, the acceptable spatial error margins for SEEG are larger than those required for anatomically driven procedures such as DBS.

The Yara system represents an advancement in robotic assistance for neurosurgery. This work demonstrates the potential of the robotic system for SEEG and paves the way for its future application in brain biopsy and DBS surgeries. The main contributions include the development of a versatile, cost-effective robotic platform, comprehensive validation using both phantom and synthetic brain models, and the integration of planning and registration methods. With continued validation and clinical trials, Yara has the potential to become widely available in hospitals, offering a safe, precise, and accessible solution for a range of neurosurgical interventions.

REFERENCES

- BEGHI, E. The epidemiology of epilepsy. **Neuroepidemiology**, S. Karger AG Basel, Switzerland, v. 54, n. 2, p. 185–191, 2020.
- BEGHI, E. *et al.* Recommendation for a definition of acute symptomatic seizure. **Epilepsia**, Wiley Online Library, v. 51, n. 4, p. 671–675, Apr 2010.
- Blausen.com staff. Medical gallery of blausen medical 2014. **WikiJournal of Medicine**, v. 1, n. 2, 2014. ISSN 2002-4436.
- BONDA, D. J. *et al.* Robot-assisted stereoelectroencephalography electrode placement in twenty-three pediatric patients: a high-resolution analysis of individual lead placement time and accuracy at a single institution. **Child's Nervous System**, Springer, v. 37, n. 7, p. 2251–2259, 2021.
- CARDINALE FRANCESCO MD, P. *et al.* Stereoelectroencephalography: Surgical methodology, safety, and stereotactic application accuracy in 500 procedures. **Neurosurgery**, v. 72, n. 3, p. 353–366, March 2013.
- DASGUPTA, D. *et al.* Previous, current, and future stereotactic eeg techniques for localising epileptic foci. **Expert Review of Medical Devices**, Taylor & Francis, v. 19, n. 7, p. 571–580, Jul 2022.
- DESSERT, G. E.; THIO, B. J.; GRILL, W. M. Optimization of patient-specific stereo-eeg recording sensitivity. **Brain Communications**, Oxford University Press US, v. 5, n. 6, p. fcad304, 2023.
- FIANI, B. *et al.* Stereoelectroencephalography versus subdural electrode implantation to determine whether patients with drug-resistant epilepsy are candidates for epilepsy surgery. **Neurol Med Chir (Tokyo)**, Neurol Med Chir, v. 61, n. 6, p. 347–355, 2021.
- FISHER, R. S. *et al.* Epileptic seizures and epilepsy: definitions proposed by the international league against epilepsy (ilae) and the international bureau for epilepsy (ibe). **Epilepsia**, Wiley Online Library, v. 46, n. 4, p. 470–472, Apr 2005.
- GAO, X. *et al.* 14 lectures on visual slam: From theory to practice. Publishing House of Electronics Industry, 2017.
- GIRGIS, F. *et al.* Superior accuracy and precision of seeg electrode insertion with frame-based vs. frameless stereotaxy methods. **Acta Neurochirurgica**, Springer, v. 162, n. 10, p. 2527–2532, 2020.
- GONZALEZ-MARTINEZ, J. *et al.* Technique, results, and complications related to robot-assisted stereoelectroencephalography. **Neurosurgery**, v. 78, p. 169–180, 2016.
- IORDANOU, J. C. *et al.* Approach angle affects accuracy in robotic stereoelectroencephalography lead placement. **World Neurosurgery**, Elsevier Inc, v. 128, p. e322–e328, 2019. ISSN 18788769. Available at: <https://doi.org/10.1016/j.wneu.2019.04.143>.

JEHI, L. *et al.* Comparative effectiveness of stereotactic electroencephalography versus subdural grids in epilepsy surgery. **Annals of neurology**, Wiley, v. 90, n. 6, p. 927–939, 2021.

JONES, J. C. *et al.* Techniques for placement of stereotactic electroencephalographic depth electrodes: Comparison of implantation and tracking accuracies in a cadaveric human study. **Epilepsia**, v. 59, p. 1667–1675, 2018. ISSN 15281167.

KAEWBORISUTSAKUL, A. *et al.* Usefulness of robotic stereotactic assistance (rosa®) device for stereoelectroencephalography electrode implantation: A systematic review and meta-analysis. **Neurologia medico-chirurgica**, The Japan Neurosurgical Society, v. 64, n. 2, p. 71–86, 2024.

KAJITA, Y. *et al.* Installation of a neuromate robot for stereotactic surgery: Efforts to conform to Japanese specifications and an approach for clinical use-technical notes. **Neurologia medico-chirurgica**, Japan Neurosurgical Society, v. 55, n. 12, p. 907–914, 2015. Available at: <https://doi.org/10.2176/nmc.tn.2015-0043>.

KIM, L. H. *et al.* Contemporaneous evaluation of patient experience, surgical strategy, and seizure outcomes in patients undergoing stereoelectroencephalography or subdural electrode monitoring. **Epilepsia**, Wiley Online Library, v. 62, n. 1, p. 74–84, 2021.

KLEIN, A. *et al.* Evaluation of 14 nonlinear deformation algorithms applied to human brain MRI registration. **NeuroImage**, Elsevier, v. 46, n. 3, p. 786–802, 2009.

LESSER, R.; CRONE, N.; WEBBER, W. Subdural electrodes. **Clin Neurophysiol**, Elsevier, v. 121, n. 9, p. 1376–1392, 2010.

LIU, L. *et al.* Frameless rosa® robot-assisted lead implantation for deep brain stimulation: technique and accuracy. **Operative Neurosurgery**, LWW, v. 19, n. 1, p. 57–64, 2020.

LOZANO, A. *et al.* **Textbook of Stereotactic and Functional Neurosurgery**. Springer, 2009. (Textbook of Stereotactic and Functional Neurosurgery, v. 1). ISBN 9783540699590. Available at: <https://books.google.com.br/books?id=cnF-2KCeR1sC>.

MAZOYER, B. In memoriam: Jean Talairach (1911–2007): a life in stereotaxy. **Human brain mapping**, v. 29, n. 2, p. 250–252, Feb 2008.

MILLER, J. W.; HAKIMIAN, S. Surgical treatment of epilepsy. **Continuum (Minneapolis Minn)**, v. 19, n. 3 Epilepsy, p. 730–742, Jun 2013.

NGUGI, A. *et al.* Estimation of the burden of active and life-time epilepsy: a meta-analytic approach. **Epilepsia**, Wiley, v. 51, n. 5, p. 883–890, 2010.

ROJAS-VILLABONA, A. *et al.* Evaluation of the stability of the stereotactic Leksell frame g in gamma knife radiosurgery. **Journal of applied clinical medical physics / American College of Medical Physics**, v. 17, p. 5944, 05 2016.

SARMAST, S. T.; ABDULLAHI, A. M.; JAHAN, N. Current classification of seizures and epilepsies: Scope, limitations and recommendations for future action. **Cureus**, Cureus Inc., v. 12, n. 9, p. e10549, 2020.

- SHEN, Y. Machine learning based epileptic seizure detection for responsive neurostimulator system optimization. **Journal of Physics: Conference Series**, v. 1453, p. 012089, 01 2020.
- SUN, C.; MOU, C. Survey on the research direction of eeg-based signal processing. **Frontiers in Neuroscience**, v. 17, 2023. ISSN 1662-453X. Available at: <https://www.frontiersin.org/journals/neuroscience/articles/10.3389/fnins.2023.1203059>.
- VASCONCELLOS, F. D. N. *et al.* Robotic-assisted stereoelectroencephalography: a systematic review and meta-analysis of safety, outcomes, and precision in refractory epilepsy patients. **Cureus**, Cureus, v. 15, n. 10, 2023.
- ZENG, B. *et al.* A surgical robot with augmented reality visualization for stereoelectroencephalography electrode implantation. **International journal of computer assisted radiology and surgery**, Springer, v. 12, n. 8, p. 1355–1368, 2017.
- ZHENG, J. *et al.* Robot-assisted versus stereotactic frame-based stereoelectroencephalography in medically refractory epilepsy. **Neurophysiologie Clinique**, Elsevier, v. 51, n. 2, p. 111–119, 2021.